HHS Public Access

Author manuscript

Nat Genet. Author manuscript; available in PMC 2013 May 01.

Published in final edited form as:

Nat Genet. 2012 November ; 44(11): 1265–1271. doi:10.1038/ng.2426.

Mutations in *CIB2*, a calcium and integrin binding protein, cause Usher syndrome type 1J and nonsyndromic deafness DFNB48

Saima Riazuddin[1,2,3,4], **Inna A. Belyantseva**[5], **Arnaud Giese**[1,2], **Kwanghyuk Lee**[6], **Artur A. Indzhykulian**[7], **Sri Pratima Nandamuri**[8], **Rizwan Yousaf**[1,9], **Ghanshyam P. Sinha**[7], **Sue Lee**[5], **David Terrell**[2], **Rashmi S. Hegde**[10], **Rana A. Ali**[9], **Saima Anwar**[9], **Paula B. Andrade-Elizondo**[6], **Asli Sirmaci**[11], **Leslie V. Parise**[12], **Sulman Basit**[13], **Abdul Wali**[14], **Muhammad Ayub**[15], **Muhammad Ansar**[13], **Wasim Ahmad**[13], **Shaheen N. Khan**[9], **Javed Akram**[16], **Mustafa Tekin**[11], **Sheikh Riazuddin**[16,17], **Tiffany Cook**[2,4,10], **Elke K. Buschbeck**[8], **Gregory I. Frolenkov**[7], **Suzanne M. Leal**[6], **Thomas B. Friedman**[5], and **Zubair M. Ahmed**[1,2,3,4,18]

[1]Division of Pediatric Otolaryngology Head & Neck Surgery, Cincinnati Children's Hospital Medical Center, Cincinnati, Ohio 45229, USA.

[2]Division of Pediatric Ophthalmology, Cincinnati Children's Hospital Medical Center, Cincinnati, Ohio 45229, USA.

[3]Department of Otolaryngology, College of Medicine, University of Cincinnati, Ohio 45229, USA.

[4]Department of Ophthalmology, College of Medicine, University of Cincinnati, Ohio 45229, USA.

[5]Laboratory of Molecular Genetics, National Institute on Deafness and Other Communication Disorders, Rockville, Maryland 20850, USA.

[6]Department of Molecular and Human Genetics, Baylor College of Medicine, Houston, Texas 77030, USA.

[7]Department of Physiology, University of Kentucky, Lexington, Kentucky 40536, USA.

[8]Department of Biological Sciences, McMicken College of Arts and Sciences, University of Cincinnati, Cincinnati, Ohio 45229, USA.

Correspondence should be addressed to Z.M.A. (zubair.ahmed@cchmc.org)..

AUTHOR CONTRIBUTIONS Z.M.A., S.R. and T.B.F. conceived and designed the study; S.R. and Z.M.A. performed linkage, RT-PCR, mutational analyses, and cloned isoforms, and provided bioinformatic evaluations; I.A.B. and S.L. conducted immunocytochemistry and quantification analyses on wild type and mutant mice inner ears, transfection assays using sensory epithelial explants and interpreted results; A.G. performed co-immunoprecipitation assays, immunocytochemistry of CIB2 in retinae and myosin VIIa mutant mice; K.L. and P.B.A.E. analyzed linkage data, and screened controls; S.B., A.W., M.A., Mu.A. and W.A. enrolled Pakistani families; G.I.F., A.A.I. and G.P.S. performed Ca^{2+} imaging in COS-7 cells, SEM imaging of zebrafish embryos and recordings of microphonic potentials; E.K.B. and S.P.N. designed and conducted ERG studies in flies; R.Y. performed morpholino microinjections, FM1-43 dye uptake, RT-PCR and startle response measurements; T.C. and D.T. generated the Cib2 mutant flies, conducted light stress analysis, light microscopic imaging of fly eyes; R.S.H. performed the molecular modeling; R.A.A., S.A., T.H., S.N.K. and Sh.R. ascertained Pakistani families, obtained clinical data, performed linkage and mutational analysis; A.S. and R.A.R. performed Cib2 immunostaining in retinae and interpreted the results; L.V.P. provided the Cib1 mutant mice; M.T. and A.S. enrolled the Turkish families and performed linkage analysis; S.M.L. supervised the work at the Baylor College of Medicine; T.B.F. supervised the work at the NIDCD/NIH and helped with data interpretation. S.R., T.B.F. and Z.M.A. wrote the manuscript; G.I.F., E.K.B., T.C., I.A.B. and S.M.L. edited the manuscript; all the authors contributed to the final version of the manuscript.

COMPETING FINANCIAL INTERESTS The authors declare no competing financial interests.

[9]National Center for Excellence in Molecular Biology, University of the Punjab, Lahore 53700, Pakistan.

[10]Division of Developmental Biology, Cincinnati Children's Hospital Medical Center, Cincinnati, Ohio 45229, USA.

[11]Department of Human Genetics, Miller School of Medicine, University of Miami, Miami, Florida 33136, USA.

[12]Department of Biochemistry & Biophysics, University of North Carolina at Chapel Hill, Chapel Hill, North Carolina 27599, USA.

[13]Department of Biochemistry, Faculty of Biological Sciences, Quaid-i-Azam University, Islamabad 45320, Pakistan.

[14]Institute of Biotechnology, Baluchistan University of Information Technology, Quetta, Pakistan.

[15]Institute of Biochemistry, University of Baluchistan, Quetta, Pakistan.

[16]Allama Iqbal Medical College, Lahore 53700, Pakistan.

[17]University of Lahore, Lahore 53700, Pakistan.

[18]Institute of Molecular Biology and Biotechnology, Bahauddin Zakariya University, Multan 60800, Pakistan.

Abstract

Sensorineural hearing loss is genetically heterogeneous. Here we report that mutations in *CIB2*, encoding a Ca^{2+}- and integrin-binding protein, are associated with nonsyndromic deafness (DFNB48) and Usher syndrome type 1J (USH1J). There is one mutation of *CIB2* that is a prevalent cause of DFNB48 deafness in Pakistan; other *CIB2* mutations contribute to deafness elsewhere in the world. In rodents, CIB2 is localized in the mechanosensory stereocilia of inner ear hair cells and in retinal photoreceptor and pigmented epithelium cells. Consistent with molecular modeling predictions of Ca^{2+} binding, CIB2 significantly decreased the ATP-induced Ca^{2+} responses in heterologous cells, while *DFNB48* mutations altered CIB2 effects on Ca^{2+} responses. Furthermore, in zebrafish and Drosophila, CIB2 is essential for the function and proper development of hair cells and retinal photoreceptor cells. We show that CIB2 is a new member of the vertebrate Usher interactome.

We previously mapped to chromosome 15q23-q25.1 a type I Usher syndrome locus (*USH1H*) segregating in two families and an autosomal recessive nonsyndromic hearing impairment (ARNSHI) locus (*DFNB48*) segregating in five families.[1,2] Subsequently, we identified 52 additional *DFNB48* families (Supplementary Figs. 1 and 2). Here we report that in affected subjects in 54 DFNB48 Pakistani families, we found a homozygous mutation (c.272T>C; p.Phe91Ser) of *CIB2* (Figs. 1 and 2a; Supplementary Fig. 3), while in two DFNB48 families (DEM4025, DEM4225) a c.297C>G (p.Cys99Trp) *CIB2* mutation co-segregated with deafness (Figs. 1 and 2a). Hence, *CIB2* is one of the major causes of ARNSHI within the Pakistani population (Supplementary Tables 1 and 2). In addition, a transition mutation c.368T>C (p.Ile123Thr) of *CIB2* co-segregated with ARNSHI in Turkish DFNB48 family 802 (Figs. 1 and 2a). SNPs linked to *CIB2* were genotyped in unrelated

affected individuals homozygous for the c.272T>C and c.297C>G mutations and the flanking haplotypes were consistent with a founder effect for both alleles (Supplementary Tables 3 and 4).

The *CIB2* gene lies distal to the critical intervals for *USH1H* locus defined by linkage analysis in family PKDF125.(ref 2) As expected, no mutations in exons of *CIB2* were found in affected members of family PKDF125. However, affected individuals in another USH1 family PKDF117 (Fig. 1c) were found to be homozygous for c.192G>C (p.Glu64Asp) in *CIB2*. This new locus is designated *USH1J*. Thus, *USH1J* and *DFNB48* are caused by allelic mutations. The four recessive mutations of *CIB2* co-segregate with deafness or deaf-blindness while carriers have normal hearing. No carriers of c.192G>C and c.368T>C were found among 676 and 724 ethnically matched control chromosomes, respectively (Supplementary Table 4). Heterozygosity for c.272T>C and c.297C>G was identified in one and five representative samples from unaffected Pakistani individuals (868 control chromosomes), respectively, but was not found in 192 individuals represented in the Coriell Human Diversity panel, in the 1000 Genome database, or in 5400 individuals listed in the NHLBI-ESP variant database (see URLs; Supplementary Table 4). Polyphen-2 (ref 3) and MutationTaster,[4] predicted that the *CIB2* mutations are deleterious (Supplementary Table 5).

CIB2 belongs to a family of calcium and integrin-binding proteins containing four EF-hand domains that change conformation upon binding Ca^{2+}, and presumably mediate intracellular Ca^{2+} signaling.[5,6] Human *CIB2* encodes three alternatively spliced isoforms, each affected by the four *USH1J/DFNB48* mutations (Fig. 2a). CIB1 is 38% identical and 59% similar to CIB2 and its crystal and NMR structures[7,8] were used to model effects of *USH1J/DFNB48* mutations (Fig. 2b-c). The three conserved residues, p.Glu64, p.Phe91 and p.Cys99 (Supplementary Fig. 4), are in a region implicated in the interaction with the C-terminal unstructured, negatively charged tail of αIIβ integrin.[7,8] These substitutions may weaken the interaction with integrin (Fig. 2b-c, Supplementary Fig. 5 and Supplementary Table 5) affecting integrin activation[9] and perhaps the efficiency of Ca^{2+} sequestering by CIB2 due to potential subtle changes in subcellular localization. In the absence of integrin, p.Arg33 (R33) forms salt bridges with p.Glu64 (E64; Fig. 2b). However, in the presence of integrin, R33 and E64 don't form a salt bridge due to a conformational change (Fig. 2c). Possibly, p.Glu64Asp alters the energetic cost of accommodating the integrin C-terminal tail affecting binding affinity or kinetics. p.Phe91 lines the effector-binding pocket, and so p.Phe91Ser may disrupt effector-binding. Similarly, substitution of tryptophan at position 99 may alter the effector-binding pocket or Ca^{2+} binding by the second EF hand domain. In contrast, p.Ile123Thr is located within the second CIB2 EF-hand neighboring p.Thr122, a Ca^{2+}-coordinating residue. Our molecular modeling predicts that p.Ile123Thr increases Ca^{2+}-binding affinity (Fig. 2b, c).

To experimentally explore the effects of these CIB2 mutations on intracellular Ca^{2+} signaling, we used ratiometric Ca^{2+} imaging to measure ATP-induced IP_3-dependent Ca^{2+} responses[10] in transiently-transfected COS-7 cells. Wild-type CIB2 decreased the sensitivity of $InsP_3$-induced Ca^{2+} release by ~40%, compared to cells transfected with an empty vector (Fig. 2d and Supplementary Fig. 6). The inhibitory effect of CIB2 on Ca^{2+} responses could be due to its Ca^{2+} buffering ability,[6] or similar to CIB1 and CaBP1, due to CIB2 interacting

with IP receptors.[10-13] 3 However, p.Cys99Trp abolished the ability of CIB2 to decrease Ca^{2+} release, while p.Ile123Thr enhanced this inhibition (Fig. 2d). This is consistent with modeling predictions of the effects of CIB2 mutations on Ca^{2+} binding affinity of CIB2. CIB2 is widely expressed in human and mouse tissues including the inner ear and retina (Supplementary Fig. 7). Transcriptome analysis revealed a 57-fold enrichment of *Cib2* mRNA in mouse cochlear hair cells at postnatal day 7 (P7) as compared to supporting cells (SHIELD, see URLs). CIB2 immunoreactivity was first observed at P2 in the organ of Corti and vestibular organs and was limited to supporting cells in the developing organ of Corti at ages up to P8 (Supplementary Fig. 8a,b). CIB2 was observed in the cytoplasm of adult supporting cells and in IHCs and OHCs cuticular plate and along the length of stereocilia (Fig. 3a-d). CIB2 staining was often brighter at shorter row stereocilia tips than the neighboring stereocilia of a longer row (Supplementary Table 6), where it may be involved in Ca^{2+} signaling that regulates mechanoelectrical transduction.[14] In adult vestibular hair cells, CIB2 was also localized along the length of stereocilia and concentrated in patches toward the tips of stereocilia (Fig. 3e, f). Gene gun transfection of auditory and vestibular hair cells with a CIB2-GFP expression vector resulted in targeting and concentration of CIB2-GFP to stereocilia tips (Fig. 3g-j). Importantly, CIB2-GFP was also more concentrated at the tips of shorter row stereocilia.

Many members of the USH-interactome bind to myosin VIIa and whirlin.[15,16] We show that CIB2 can multimerize and interacts with whirlin, which is localized at the tips of stereocilia,[17] and myosin VIIa (Fig. 4 and Supplementary Fig. 9). No interaction of CIB2 was found with the other reported USH proteins. Thus CIB2 is a member of the USH-interactome (Supplementary Fig. 10). To explore if myosin VII or whirlin are necessary for CIB2 localization at hair cell stereocilia tips we immunostained homozygous shaker 1 (*Myo7a*^{4626sb}) and *whirler* (*whrn*) mice organ of Corti using CIB2 antibody. We observe no mislocalization of CIB2 in stereocilia of homozygous *Myo7a* and *whrn* mutant mice (Supplementary Figs. 8i-p, 11), indicating that *in vivo*, myosin VIIa and whirlin are not required for localization of CIB2 in mouse inner ear hair cell stereocilia.

We next probed the function of CIB2 in the sensory cells of the ear and eye, which we studied in zebrafish where *zcib2* (NM_200706.1) is expressed throughout development (Supplementary Fig. 12a). Using anti-*cib2* specific morpholinos, we knocked down z*cib2* in embryos (Supplementary Figs. 12b and 13). We categorized the phenotypes at 72 hours post-fertilization (hpf) into class I (normal like), class II (tail defect), class III (tail defect, micro-ophthalmia, blood pooling) and class IV (hypo-pigmentation, micro-ophthalmia, tail defects and retarded development; Fig. 5a-b). Approximately 80% of 5-day-old morphants did not respond to acoustic stimuli or were unable to remain upright while swimming (Fig. 5c). Scanning electron microscopy revealed a dramatic decrease in the number of neuromasts in morphants (Fig. 5d-k). However, among class I and II-morphants, we found some neuromasts with hair cell bundles (Fig. 5f-i and Supplementary Fig. 14). To assess the functional status of neuromast hair cells in the lateral lines, we briefly exposed larvae to FM1-43, a styryl pyridinium dye, which enters the hair cells via partially open MET channels at rest[18-21], or its fixable analog AM1-43. Controls showed prominent fluorescent hair cell patches (neuromasts) at the head and lateral line regions (Fig. 5l). Morphants had

few or no fluorescent neuromasts at 96 hpf (Fig. 5l). We measured the microphonic potentials of these neuromasts and, consistent with the FM1-43 dye uptake, we observed reduction in extracellular receptor potentials (Fig. 5m-o), which could be a result of nonfunctional or degenerating MET components in lateral line hair cells. Thus, CIB2 function is essential for development, maintenance, and/or function of the mechanosensory hair cells in zebrafish.

In the mammalian inner ear, an optimal intracellular Ca^{2+} concentration is critical for MET, adaptation, frequency tuning, hair bundle twitching, outer hair cell electromotility, and afferent synaptic transmission.[22-32] Ca^{2+} levels in stereocilia rely on mobile Ca^{2+} buffers, a mitochondria belt beneath the cuticular plate, and PMCA, a Ca^{2+}-ATPase.[14,22,33-35] Hair cell bundles of both cochlear and vestibular organs differentially express various calcium-binding proteins including calmodulin, calretinin, parvalbumin and calbindin-D28K,[33,36-42] mobile buffers that help maintain an optimal Ca^{2+} concentration. Based on stereocilia tip localization, one may hypothesize that CIB2 temporarily sequesters Ca^{2+} entering the stereocilia through MET channels until Ca^{2+} exits the stereocilia through PMCA,[35,43-46] or is taken up by mitochondria beneath the cuticular plate. Another plausible non mutually exclusive function of CIB2 is the maintenance of Ca^{2+} homeostasis in the hair cell body, which in turn may modulate the OHC electromotility.[28,29,47] Furthermore, CIB2 is also concentrated in the cuticular plate region of hair cells where an ATP-gated IP_3-dependent intracellular Ca^{2+} store is located.[12] Similar to CaBP1, CIB2 may interact directly with IP3 receptors,[10] modulating purinergic responses in OHCs.[12] The analysis of hair cell physiology in a CIB2 mutant mouse would help clarify and distinguish between some of these hypotheses. To gain insight into the function of CIB2 in the mammalian eye, we determined the localization of CIB2 in the mouse retina. CIB2 immunoreactivity was observed in inner and outer segments of photoreceptor cells as well as in the retinal-pigmented epithelium (RPE). Diffuse immunoreactivity was also observed in the inner (IPL) and outer plexiform layers (OPL) and ganglion cell layer (Supplementary Fig. 15).

The Drosophila genome encodes one CIB-related gene, *CG9236*, which shares similarity to human CIB2 (59% identity). *CG9236* (*dCib2*) is expressed in several tissues, including the adult eye.[48] Calcium levels control many aspects of Drosophila phototransduction.[49,50] To further assess CIB2 function, we measured phototransduction activity with electroretinograms (ERGs) following *dCib2* RNAi-knockdown. $dCib2^{RNAi}$ flies showed significantly reduced photoresponse amplitude (Fig. 6a, b) and impaired responses to flicker stimuli at high frequencies (Fig 6c, d). $dCib2^{RNAi}$ flies failed to reliably follow individual pulses by ~40 Hz, whereas controls only exhibited this behavior by ~70Hz (Fig 6c). $dCib2^{RNAi}$ response amplitudes to individual flicker stimuli also approached noise levels at lower frequencies than those of controls (Fig 6d). Finally, $dCib2^{RNAi}$ flies failed to sustain an adequate photoresponse during prolonged stimulation, even at a low frequency of 1.7Hz (Fig 6e, f). Collectively, these data indicate that *dCib2* is necessary to achieve a strong, sustained photoresponse and to track fast light stimuli, phenotypes consistent with transiently elevated intracellular Ca^{2+} concentrations.[49,50]

Since calcium dysregulation is associated with retinitis pigmentosa and light-induced retinal degeneration,[50] we analyzed photoreceptor morphology in $dCib2^{RNAi}$ Drosophila. Control

and *dCib2*^{RNAi} flies showed no obvious eye dysmorphology when raised under 12 hr:12 hr light-dark conditions (Fig. 6g). However, *dCib2*^{RNAi} flies exhibited significant photoreceptor degeneration when raised under constant light for 5 days (Fig. 6g). Thus, dCib2 is required for proper phototransduction and prevention of light-dependent retinal degeneration. These physiological and morphological phenotypes are consistent with the presence of an elevated intracellular Ca^{2+} concentration,[49,50] which inhibits PLC that normally activates cation-permeable TRP channels opening in response to light.[51] High levels of intracellular Ca^{2+} are also known to inactivate TRP channels, and hence reduce the photoresponse.[51] Several previous studies have indicated that proper calcium regulation and phototransduction are necessary to maintain photoreceptor integrity, and defects in calcium regulation are particularly sensitive to light-induced photoreceptor degeneration.[49,50]

In summary, *CIB2* mutations underlie Usher syndrome 1J and nonsyndromic deafness DFNB48. Since CIB2 is concentrated in stereocilia and interacts with myosin VIIa and whirlin, and *Cib2* morphants have reduced hair cell microphonic potential, we speculate that CIB2 participates in Ca^{2+} regulation of the mechanotransduction process. Our studies reveal that, as in humans, Drosophila Cib2 is critical for proper photoreceptor maintenance and function, and that CIB2 plays conserved roles in calcium homeostasis.

URLs

NHLBI-ESP variant database, http://evs.gs.washington.edu/EVS/;

SHIELD, https://shield.hms.harvard.edu/viewgene.html?gene=Cib2;

Primer3, http://frodo.wi.mit.edu/;

1000 Genome, browser.1000genomes.org/;

Polyphen-2, http://genetics.bwh.harvard.edu/pph2/index.shtml;

Mutation Taster, http://www.mutationtaster.org/;

Project HOPE, http://www.cmbi.ru.nl/hope/modeling;

Yasara, http://www.yasara.org/.

METHODS

Subject and clinical evaluations

This study was approved by IRBs at the National Centre of Excellence in Molecular Biology (NCEMB), Lahore, Pakistan (FWA00001758), at the National Institutes of Health, USA (Combined Neuroscience IRB; OH-93-N-016), at the Cincinnati Children's Hospital Research Foundation, USA (2009-0684; 2010-0291), at the Baylor College of Medicine, USA, at the University of Miami, and at Quaid-i-Azam University, Islamabad, Pakistan. Written informed consent was obtained from adult subjects and parents of minor subjects. The degree of HI was assessed by pure tone air conduction audiometry at frequencies ranging from 250 to 8000 Hz. Vestibular function was evaluated by tandem gait and

Romberg testing. Funduscopic and electroretinographic examinations were performed on 14 affected individuals from DFNB48 families and two affected individuals from the USH1J family (PKDF117) by an ophthalmologist to detect the absence or presence of frank retinopathy.[1,2] Peripheral blood samples or buccal swabs for genomic DNA extraction were collected from participating subjects.

Genetic linkage and mutation analysis studies

Using genomic DNA from affected members of two USH1 and five DFNB48 families (Supplementary Table 2), we sequenced ~100 bp of adjacent intronic sequence flanking all exons of the 16 candidate genes. *CIB2* primers are listed in Supplementary Table 7. Methods for direct sequencing and mutational analyses were described.[53] Control DNA samples from ethnically matched Pakistani, Turkish, and Coriell Human Diversity and Caucasian populations were sequenced for mutations of *CIB2*.

Molecular modeling

Two homology models of CIB2 were constructed; the templates were the high resolution crystal structure of human CIB1 (1XO5A.PDB),[5] and the solution structure of a Ca^{2+}-CIB1 complex (Fig. 2b) with the cytoplasmic domain of the integrin αIIβ subunit (2LM5.PDB).[8] The SWISS-MODEL server[54] was used for modeling, and energy minimization and analysis were done with Yasara (see URLs.). We also used the Project HOPE web server to further determine the effect of missense mutations on the structure of CIB2.[55]

Calcium imaging

COS-7 cells were transfected with various DsRed-tagged constructs using Lipofectamine 2000 and 3-4 μg of DNA per ~1ml of serum-free Opti-MEM medium (Invitrogen). 20-28 hours post-transfection, cells were loaded with 18 μM of ratiometric Ca^{2+} indicator, Fura-2 AM (Molecular Probes) for 1-1.5 h at room temperature. Fura-2 fluorescence was observed in L-15 medium at room temperature with sequential 340 and 380 nm illuminations at a rate of 0.78-0.81 image pairs per second. The F_{340}/F_{380} ratio images were calculated and pixel values were converted to intracellular Ca^{2+} concentration using calibration curve obtained with Fura-2 Calibration Kit (Molecular Probes). Ca^{2+}-responses were evoked by application of 1 μM of ATP for 50 sec through a puff pipette of ~1 μm diameter situated at ~25 μm from the cell (Supplementary Fig. 6). The number of dishes used for every construct was 4 or greater and the number of transfected cells for every construct was over 40.

Qualitative and relative quantitative RT-PCR analysis

For PCR-based expression analyses, we used cDNA panels (Clontech) produced from tissues obtained from 19 to 69 year old human and from 8 to 12 weeks old mice. Gene-specific primers were used in exons 1 and 5 of *Cib2*. For relative quantitative analysis of *Cib2*, the PCR primers were located in exons 4 and 5, while the Taqman probe spanned the junction of exons 4 and 5.

Fluorescently-tagged expression constructs

We used PCR-ready adult human eye cDNA (Clontech) for cloning the full-length isoform of CIB2 into GFP and tdTomato (Clontech) tagged vectors (Supplementary Fig. 16). Mouse full-length *Cib2* cDNA was PCR amplified from postnatal day 1 (P1) to P5 inner ear cDNA. For expression plasmids, both strands of the cDNA inserts were verified with Sanger sequencing. Full-length and deletion constructs of mouse whirlin have been described previously.[17]

Antibody validation

To validate anti-CIB2 antibody (H00010518-A01, Abnova), we performed a co-localization assay using CIB2-GFP, DsRed-CIB1, GFP-CIB3 and GFP-CIB4 transfected COS-7 cells (Supplementary Fig. 16). Transfected by electroporation (Neon, Invitrogen) COS-7 cells were incubated overnight at 37°C with 5% CO2 and then fixed with 4% paraformaldehyde (EMS) for 20 min, permeabilized for 15 min in 0.2% Triton X-100 and blocked by incubation in 2% BSA and 5% normal goat serum for 30 min. All solutions were made with 1XPBS. Then COS-7 cells were incubated with CIB2 antibody diluted with blocking solution to a concentration of ~5 μg/ml and incubated for 2 hrs. After washes, Alexa Fluor 568 goat anti-rabbit IgG (Molecular Probes) diluted 1:500 were used for 20 min at room temperature. Samples were mounted using ProLong Gold Antifade Reagent (Molecular Probes), and imaged on a LSM780 confocal microscope equipped with a Zeiss 63X, 1.4 N.A. objective.

Immunostaining

C57BL6/J, *shaker 2* (*Myo15a*^{sh2}) and *whirler* (*Whrn*) mutant mice were handled according to the NIH protocol 1263-09. Inner ears were dissected and immunostained as described[17] with slight modifications. Tissue was fixed in 4% paraformaldehyde in 1xPBS (with Ca^{2+} and Mg^{2+}) overnight at 4°C. All other reagents, including anti-CIB2 antibody used at 1:200 dilution and Alexa 488 IgG (Invitrogen), were diluted in 1XPBS supplemented with 2mM EDTA. Samples were mounted with ProLong Gold Antifade Reagent and imaged using LSM780 equipped with a 63× 1.4 N.A. objective (Zeiss Microimaging Inc.). Sensory epithelium of the retina was dissected from adult CD1 mice, stained with the CIB2 antibody, and imaged using the LSM700 system. Fluorescence intensity of CIB2 labeling at stereocilia tips of P13 and P31 *C57Bl/6J*, P11 *Whrn*$^{+/wi}$, and P31*Myo7a* $^{+/4626sb}$ mice were measured using Image J. The region of interest (ROI) covered tips of either first (tallest) or second rows of stereocilia from individual stereocilia bundles of inner hair cells. The integrated intensity of fluorescence was measured within these ROIs at the focal planes where stereocilia tips were in best focus. These valeues were then divided by the number of stereocilia within the corresponding ROIs to determine the labeling intensity per stereocilium. The amounts of CIB2 labeling at different stereocilia rows were compared using an unpaired *t*-test.

Helios gene gun transfection

P2-P3 organ of Corti and vestibular sensory epithelial explants of C57Bl/6, *shaker-2* and *Whrn* mutant mice were cultured for one day in DMEM media supplemented by 7% FBS at

37°C with 5% CO_2 and transfected with CIB2-GFP expression construct using a Helios gene gun as described.[56] After 24-48 h post-transfection, cultures were fixed in 4% paraformaldehyde overnight at 4°C and stained with rhodamine-phalloidin as described.[17] Then samples were mounted with ProLong Gold Reagent and imaged using LSM780 system equipped with 63× 1.4 N.A. objective (Zeiss Microimaging Inc.).

Co-immunoprecipitation assay

HEK293 cells (ATCC) were maintained using DMEM supplemented with 10% fetal bovine serum (Invitrogen), glutamine and penicillin-streptomycin (Invitrogen). Cells were plated at 80% confluency for 24 hours at 37°C/5% CO_2. On the day of transfection, 10ug of each DNA were transfected using the Fugene HD Kit. Forty-eight hours after transfection, cells were homogenized with a sonicator (Fisher Scientific) at intensity setting 2 for 10s in buffer A (50 mM Tris-HCl pH 7.5, 100 mM NaCl, 1% NP-40) containing a protease inhibitor mixture (Roche). Protein A-Sepharose CL-4B beads were incubated 4 hours with 5ug of anti-GFP antibody and washed three times with PBS containing 0.1% Triton X-100. Lysates were incubated 16h with protein A-Sepharose CL-4B beads and centrifuged at 10,000 g for 3 min. Protein A-Sepharose CL-4B beads (Roche) were washed with buffer A three times, and boiled in 2x SDS sample buffer.

Zebrafish Morpholino injections and fluorescent staining

A *zcib2* translation blocking specific morpholino (7.5 ng; Supplementary Table 7) or splice junction site specific morpholino (10 ng) and a control morpholino (scrambled sequence) was injected at the one cell stage as described.[57] Fluorescent labeling of lateral line neuromasts with 3 μM AM1-43 was performed as described.[21] The translational and splice site morpholinos against *cib2* resulted in an identical phenotype.

Startle response assays

Five day old *zcib2*-morphants and control larvae were placed into a 10-cm-diameter dishes and allowed to acclimate for 10 min before being tested. The startle reflex was video-recorded using a digital camera after larvae were stimulated with a series of taps on the edge of the dish as previously described.[58]

Zebrafish scanning electron microscopy

zcib2-morphants and control mock-transfected larvae were fixed in 2.5% glutaraldehyde in 0.1M cacodylate buffer supplemented with 2 mM $CaCl_2$ for 1-2 hours at room temperature. The specimens were dehydrated in a graded series of ethanol, critical-point dried from liquid CO_2, sputter-coated with platinum (5.0 nm, controlled by a film-thickness monitor), and observed with a field-emission SEM (S-4800, Hitachi, Japan).

Recordings of microphonic potential in zebrafish

Zebrafish larvae were anesthetized using 0.01% MS-222 (Tricaine; Sigma) dissolved in a normal bath solution containing the following inorganic salts (in mM): NaCl (120), KCl (2), HEPES (10), $CaCl_2$ (2), and NaH_2PO_4 (0.7). pH and supplemented with 150 nM of tetrodotoxin (Sigma) to reduce muscle twitching. The larva were secured on glass bottom

dish with nylon fibers. The microphonic potentials were recorded at room temperature (22°C) using borosilicate glass electrodes with the resistance of 5-6 MΩ that were placed near the apical edges of the lateral line neuromasts. We recorded from posterior neuromasts that had healthy looking hair cells. Kinocilia tufts were deflected with a stiff glass probe driven by a piezoelectric actuator (PA 8/12, Piezosystem Jena, Germany) with sinusoidal stimuli of 2 μm peak-to-peak amplitude at 100 Hz. Microphonic potentials were recorded with an Axopatch 200B (Molecular Devices) amplifier in a current-clamp mode, further amplified by 10x (SIM983, Stanford research), and low-pass filtered at 1-2 kHz. All records represent an average of 1000 responses.

Drosophila genetics and morphogenesis studies

Transgenic lines carrying a UAS-driven hairpin RNAi construct for *CG9236* (ref 59) on the II and III chromosome were obtained from the Vienna Drosophila RNAi Center (VDRC). These flies were crossed to a recombined chromosome carrying three transgenes - pWIZ, UAS-Dicer2, long-GMR-GAL4flies. pWIZ is an RNAi line that diminishes expression of *w* gene (white eye), thus reducing autofluorescent pigmentation,[60] Dicer 2 increases efficiency of RNAi-mediated knockdown,[59] and long-GMR-GAL4 drives UAS-dependent gene expression specifically in differentiated cells in the eye.[61] Flies were maintained on standard agar/cornmeal/molasses media at 25°C. For the light-induced degeneration studies, flies were raised in standard polystyrene fly vials 12 inches from a 25-watt fluorescent light bulb for 5 days (Applied Scientific). Photoreceptor morphology was monitored in live flies using a water-immersion, cornea neutralization, epifluorescence procedure previously described.[62] We verified photoreceptor morphology using 2 μm plastic sections of dissected retinas, counterstained with toluidine blue (Sigma), as previously described.[63] Ten to twelve flies were examined per experimental group, and the light-dependent degeneration assay was conducted three times.

Electroretinogram (ERG) recordings in *Drosophila*

Flies were immobilized with CO_2, mounted on a cover slip with pink dental wax (Electron Microscopy Sciences) and dark-adapted. The recording electrode (a cotton wick containing 0.9% NaCl w/v connected to a silver wire) was positioned on the surface of the eye, and the indifferent electrode (silver wire) in the abdomen. Recordings were acquired at 10,000 Hz. White light stimuli (with an intensity of 1.70×10^{-14} photons/cm^2/sec) were delivered through an optical fiber connected to an LED. Data was analyzed in MATLAB (MathWorks, Inc., Natick, MA, USA). All data was smoothed with [filter{ones(1,windowsize)/windowsize,1,data}] with the following window sizes: Amplitude: 5 sec stimuli 1000; 300 ms stimuli 100; Frequency: 10% of cycle length, Sustainability: 100. To establish the amplitude, the absolute voltage difference between baseline and maximal response was averaged over approximately 20 pulses per fly. To establish the response amplitudes to individual flicker frequencies, each cycle's maximum and following minimum response was established, and the absolute value of their difference was averaged for pulses 11-23. Sustainability was tested with a train of 150 300ms pulses at 1.7Hz. Noise levels are based on baseline data.

Supplementary Material

Refer to Web version on PubMed Central for supplementary material.

ACKNOWLEDGMENTS

We thank the families for their participation and cooperation. We also thank Drs. G. N. Sarangdhar, R. Rachel, T. Jaworek, V. Ponferrada and K. Gul for technical assistance and Drs. R. J. Morell, J. Schultz, D. Drayna, A. Swaroop and A.J. Griffith for critique of the manuscript. We also thank Tina M. Leisner at University of North Carolina for the generous gift of CIB antibodies. Genotyping services were provided to S.M.L. by the Center for Inherited Disease Research (CIDR). CIDR is fully funded through a federal contract (N01-HG-65403) from the NIH to Johns Hopkins University. Z.M.A. is a recipient of a RPB Career Development Award. This work was also supported by the Higher Education Commission and Ministry of Science and Technology, Islamabad, Pakistan, to Sh.R. and W.A.; the International Center for Genetic Engineering and Biotechnology, Trieste, Italy under project CRP/PAK08-01 contract no. 08/009 to Sh.R.; Cincinnati Children's Hospital Research Foundation (CCHMC) Intramural Research Funds, to S.R. and Z.M.A.; National Institute on Deafness and Other Communication Disorders (NIDCD/NIH) research grants R01 DC03594 and DC011651 to S.M.L.; R01 HL092544 to L.V.P.; R01 DC009645 to M.T.; R01 DC008861 to G.I.F.; R01 DC012564 and R00 DC009287 to Z.M.A.; R01 DC011803 and R01 DC011748 to S.R. and intramural funds from NIDCD DC000039-15 to T.B.F.

REFERENCES

1. Ahmad J, et al. DFNB48, a new nonsyndromic recessive deafness locus, maps to chromosome 15q23-q25.1. Hum Genet. 2005; 116:407–12. [PubMed: 15711797]
2. Ahmed ZM, Riazuddin S, Khan SN, Friedman PL, Friedman TB. USH1H, a novel locus for type I Usher syndrome, maps to chromosome 15q22-23. Clin Genet. 2009; 75:86–91. [PubMed: 18505454]
3. Adzhubei IA, et al. A method and server for predicting damaging missense mutations. Nature methods. 2010; 7:248–9. [PubMed: 20354512]
4. Schwarz JM, Rodelsperger C, Schuelke M, Seelow D. MutationTaster evaluates disease-causing potential of sequence alterations. Nature methods. 2010; 7:575–6. [PubMed: 20676075]
5. Gentry HR, et al. Structural and biochemical characterization of CIB1 delineates a new family of EF-hand-containing proteins. J Biol Chem. 2005; 280:8407–15. [PubMed: 15574431]
6. Blazejczyk M, et al. Biochemical characterization and expression analysis of a novel EF-hand Ca2+ binding protein calmyrin2 (Cib2) in brain indicates its function in NMDA receptor mediated Ca2+ signaling. Arch Biochem Biophys. 2009; 487:66–78. [PubMed: 19433056]
7. Huang H, Ishida H, Yamniuk AP, Vogel HJ. Solution structures of Ca2+-CIB1 and Mg2+-CIB1 and their interactions with the platelet integrin alphaIIb cytoplasmic domain. The Journal of biological chemistry. 2011; 286:17181–92. [PubMed: 21388953]
8. Huang H, Vogel HJ. Structural basis for the activation of platelet integrin alphaIIbbeta3 by calcium- and integrin-binding protein 1. Journal of the American Chemical Society. 2012; 134:3864–72. [PubMed: 22283712]
9. Hager M, et al. Cib2 binds integrin alpha7Bbeta1D and is reduced in laminin alpha2 chain-deficient muscular dystrophy. J Biol Chem. 2008; 283:24760–9. [PubMed: 18611855]
10. Kasri NN, et al. Regulation of InsP3 receptor activity by neuronal Ca2+-binding proteins. EMBO J. 2004; 23:312–21. [PubMed: 14685260]
11. Hennigs JK, et al. Sweet taste receptor interacting protein CIB1 is a general inhibitor of InsP3-dependent Ca2+ release in vivo. Journal of neurochemistry. 2008; 106:2249–62. [PubMed: 18627437]
12. Mammano F, et al. ATP-Induced Ca(2+) release in cochlear outer hair cells: localization of an inositol triphosphate-gated Ca(2+) store to the base of the sensory hair bundle. J Neurosci. 1999; 19:6918–29. [PubMed: 10436049]
13. White C, Yang J, Monteiro MJ, Foskett JK. CIB1, a ubiquitously expressed Ca2+-binding protein ligand of the InsP3 receptor Ca2+ release channel. The Journal of biological chemistry. 2006; 281:20825–33. [PubMed: 16723353]

14. Beurg M, Nam JH, Chen Q, Fettiplace R. Calcium balance and mechanotransduction in rat cochlear hair cells. J Neurophysiol. 2010; 104:18–34. [PubMed: 20427623]
15. Reiners J, Nagel-Wolfrum K, Jurgens K, Marker T, Wolfrum U. Molecular basis of human Usher syndrome: deciphering the meshes of the Usher protein network provides insights into the pathomechanisms of the Usher disease. Exp Eye Res. 2006; 83:97–119. [PubMed: 16545802]
16. van Wijk E, et al. The DFNB31 gene product whirlin connects to the Usher protein network in the cochlea and retina by direct association with USH2A and VLGR1. Hum Mol Genet. 2006; 15:751–65. [PubMed: 16434480]
17. Belyantseva IA, et al. Myosin-XVa is required for tip localization of whirlin and differential elongation of hair-cell stereocilia. Nat Cell Biol. 2005; 7:148–56. [PubMed: 15654330]
18. Gale JE, Marcotti W, Kennedy HJ, Kros CJ, Richardson GP. FM1-43 dye behaves as a permeant blocker of the hair-cell mechanotransducer channel. J Neurosci. 2001; 21:7013–25. [PubMed: 11549711]
19. Meyers JR, et al. Lighting up the senses: FM1-43 loading of sensory cells through nonselective ion channels. J Neurosci. 2003; 23:4054–65. [PubMed: 12764092]
20. Seiler C, et al. Myosin VI is required for structural integrity of the apical surface of sensory hair cells in zebrafish. Dev Biol. 2004; 272:328–38. [PubMed: 15282151]
21. Seiler C, Nicolson T. Defective calmodulin-dependent rapid apical endocytosis in zebrafish sensory hair cell mutants. J Neurobiol. 1999; 41:424–34. [PubMed: 10526320]
22. Lumpkin EA, Hudspeth AJ. Regulation of free Ca2+ concentration in hair-cell stereocilia. J Neurosci. 1998; 18:6300–18. [PubMed: 9698322]
23. Denk W, Holt JR, Shepherd GM, Corey DP. Calcium imaging of single stereocilia in hair cells: localization of transduction channels at both ends of tip links. Neuron. 1995; 15:1311–21. [PubMed: 8845155]
24. Fettiplace R, Ricci AJ. Adaptation in auditory hair cells. Curr Opin Neurobiol. 2003; 13:446–51. [PubMed: 12965292]
25. Brandt A, Striessnig J, Moser T. CaV1.3 channels are essential for development and presynaptic activity of cochlear inner hair cells. J Neurosci. 2003; 23:10832–40. [PubMed: 14645476]
26. Fuchs PA, Glowatzki E, Moser T. The afferent synapse of cochlear hair cells. Curr Opin Neurobiol. 2003; 13:452–8. [PubMed: 12965293]
27. Dulon D, Zajic G, Schacht J. Increasing intracellular free calcium induces circumferential contractions in isolated cochlear outer hair cells. J Neurosci. 1990; 10:1388–97. [PubMed: 2109787]
28. Dallos P, et al. Acetylcholine, outer hair cell electromotility, and the cochlear amplifier. J Neurosci. 1997; 17:2212–26. [PubMed: 9045745]
29. Frolenkov GI, Mammano F, Belyantseva IA, Coling D, Kachar B. Two distinct Ca(2+)-dependent signaling pathways regulate the motor output of cochlear outer hair cells. J Neurosci. 2000; 20:5940–8. [PubMed: 10934241]
30. Benser ME, Marquis RE, Hudspeth AJ. Rapid, active hair bundle movements in hair cells from the bullfrog's sacculus. J Neurosci. 1996; 16:5629–43. [PubMed: 8795619]
31. Hudspeth AJ. Hair-bundle mechanics and a model for mechanoelectrical transduction by hair cells. Soc Gen Physiol Ser. 1992; 47:357–70. [PubMed: 1369770]
32. Eatock RA, Corey DP, Hudspeth AJ. Adaptation of mechanoelectrical transduction in hair cells of the bullfrog's sacculus. J Neurosci. 1987; 7:2821–36. [PubMed: 3498016]
33. Ricci AJ, Wu YC, Fettiplace R. The endogenous calcium buffer and the time course of transducer adaptation in auditory hair cells. J Neurosci. 1998; 18:8261–77. [PubMed: 9763471]
34. Wood JD, Muchinsky SJ, Filoteo AG, Penniston JT, Tempel BL. Low endolymph calcium concentrations in deafwaddler2J mice suggest that PMCA2 contributes to endolymph calcium maintenance. J Assoc Res Otolaryngol. 2004; 5:99–110. [PubMed: 15357414]
35. Yamoah EN, et al. Plasma membrane Ca2+-ATPase extrudes Ca2+ from hair cell stereocilia. J Neurosci. 1998; 18:610–24. [PubMed: 9425003]

36. Baird RA, Steyger PS, Schuff NR. Intracellular distributions and putative functions of calcium-binding proteins in the bullfrog vestibular otolith organs. Hear Res. 1997; 103:85–100. [PubMed: 9007577]
37. Walker RG, Hudspeth AJ, Gillespie PG. Calmodulin and calmodulin-binding proteins in hair bundles. Proc Natl Acad Sci U S A. 1993; 90:2807–11. [PubMed: 8385344]
38. Hackney CM, Mahendrasingam S, Penn A, Fettiplace R. The concentrations of calcium buffering proteins in mammalian cochlear hair cells. J Neurosci. 2005; 25:7867–75. [PubMed: 16120789]
39. Dechesne CJ, et al. Identification and ultrastructural localization of a calretinin-like calcium-binding protein (protein 10) in the guinea pig and rat inner ear. Brain Res. 1991; 560:139–48. [PubMed: 1722130]
40. Yang D, Thalmann I, Thalmann R, Simmons DD. Expression of alpha and beta parvalbumin is differentially regulated in the rat organ of corti during development. J Neurobiol. 2004; 58:479–92. [PubMed: 14978725]
41. Sakaguchi N, Henzl MT, Thalmann I, Thalmann R, Schulte BA. Oncomodulin is expressed exclusively by outer hair cells in the organ of Corti. J Histochem Cytochem. 1998; 46:29–40. [PubMed: 9405492]
42. Hackney CM, Mahendrasingam S, Jones EM, Fettiplace R. The distribution of calcium buffering proteins in the turtle cochlea. J Neurosci. 2003; 23:4577–89. [PubMed: 12805298]
43. Dumont RA, et al. Plasma membrane Ca2+-ATPase isoform 2a is the PMCA of hair bundles. J Neurosci. 2001; 21:5066–78. [PubMed: 11438582]
44. Hill JK, et al. Splice-site A choice targets plasma-membrane Ca2+-ATPase isoform 2 to hair bundles. J Neurosci. 2006; 26:6172–80. [PubMed: 16763025]
45. Silverstein RS, Tempel BL. Atp2b2, encoding plasma membrane Ca2+-ATPase type 2, (PMCA2) exhibits tissue-specific first exon usage in hair cells, neurons, and mammary glands of mice. Neuroscience. 2006; 141:245–57. [PubMed: 16675132]
46. Street VA, McKee-Johnson JW, Fonseca RC, Tempel BL, Noben-Trauth K. Mutations in a plasma membrane Ca2+-ATPase gene cause deafness in deafwaddler mice. Nat Genet. 1998; 19:390–4. [PubMed: 9697703]
47. Jones SM, et al. Stimulus and recording variables and their effects on mammalian vestibular evoked potentials. J Neurosci Methods. 2002; 118:23–31. [PubMed: 12191754]
48. Chintapalli VR, Wang J, Dow JA. Using FlyAtlas to identify better Drosophila melanogaster models of human disease. Nature genetics. 2007; 39:715–20. [PubMed: 17534367]
49. O'Tousa JE. Ca2+ regulation of Drosophila phototransduction. Advances in experimental medicine and biology. 2002; 514:493–505. [PubMed: 12596941]
50. Wang T, Montell C. Phototransduction and retinal degeneration in Drosophila. Pflugers Archiv : European journal of physiology. 2007; 454:821–47. [PubMed: 17487503]
51. Gu Y, Oberwinkler J, Postma M, Hardie RC. Mechanisms of light adaptation in Drosophila photoreceptors. Current biology : CB. 2005; 15:1228–34. [PubMed: 16005297]
52. Nicolson T, et al. Genetic analysis of vertebrate sensory hair cell mechanosensation: the zebrafish circler mutants. Neuron. 1998; 20:271–83. [PubMed: 9491988]
53. Riazuddin S, et al. Tricellulin is a tight-junction protein necessary for hearing. American journal of human genetics. 2006; 79:1040–51. [PubMed: 17186462]
54. Arnold K, Bordoli L, Kopp J, Schwede T. The SWISS-MODEL workspace: a web-based environment for protein structure homology modelling. Bioinformatics. 2006; 22:195–201. [PubMed: 16301204]
55. Venselaar H, Te Beek TA, Kuipers RK, Hekkelman ML, Vriend G. Protein structure analysis of mutations causing inheritable diseases. An e-Science approach with life scientist friendly interfaces. BMC bioinformatics. 2010; 11:548. [PubMed: 21059217]
56. Belyantseva IA. Helios Gene Gun-mediated transfection of the inner ear sensory epithelium. Methods in molecular biology. 2009; 493:103–23. [PubMed: 18839344]
57. Nasevicius A, Ekker SC. Effective targeted gene 'knockdown' in zebrafish. Nature genetics. 2000; 26:216–20. [PubMed: 11017081]

58. Sidi S, Friedrich RW, Nicolson T. NompC TRP channel required for vertebrate sensory hair cell mechanotransduction. Science. 2003; 301:96–9. [PubMed: 12805553]
59. Dietzl G, et al. A genome-wide transgenic RNAi library for conditional gene inactivation in Drosophila. Nature. 2007; 448:151–6. [PubMed: 17625558]
60. Lee YS, Carthew RW. Making a better RNAi vector for Drosophila: use of intron spacers. Methods. 2003; 30:322–9. [PubMed: 12828946]
61. Wernet MF, et al. Homothorax switches function of Drosophila photoreceptors from color to polarized light sensors. Cell. 2003; 115:267–79. [PubMed: 14636555]
62. Pichaud F, Desplan C. A new visualization approach for identifying mutations that affect differentiation and organization of the Drosophila ommatidia. Development. 2001; 128:815–26. [PubMed: 11222137]
63. Charlton-Perkins M, et al. Prospero and Pax2 combinatorially control neural cell fate decisions by modulating Ras- and Notch-dependent signaling. Neural development. 2011; 6:20. [PubMed: 21539742]

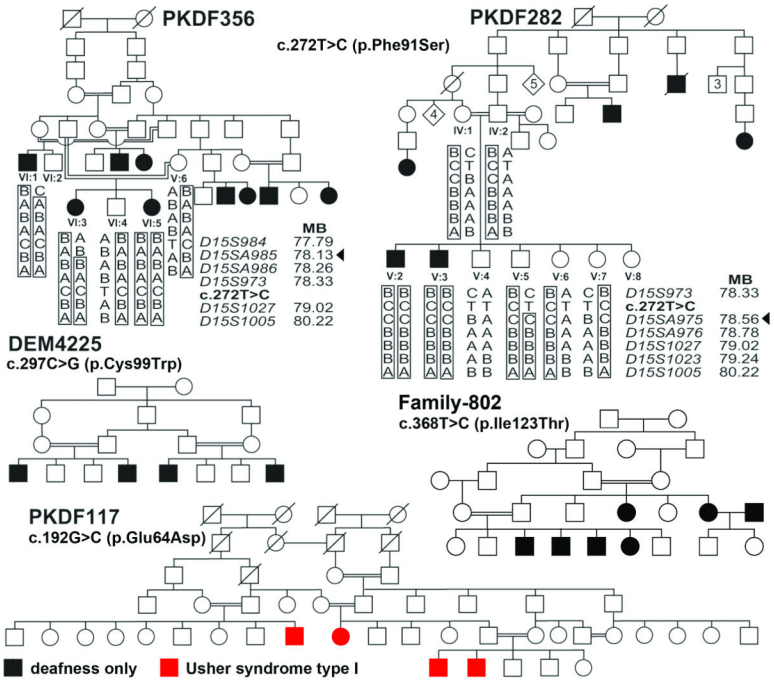

Figure 1.

Pedigrees of USH1J/DFNB48 families. One USH1J and four of 57 NSHI DFNB48 families segregating *CIB2* (NM_006383) mutant alleles. Filled symbols represent affected individuals and a double horizontal line is a consanguineous marriage. Haplotypes for selected individuals of families PKDF356 and PKDF282 indicate the smallest linkage interval. The proximal breakpoint (arrow) is defined by affected individual VI:3 of family PKDF356 at marker *D15SA985* (78.13 Mb). The distal breakpoint (arrowhead) is defined by unaffected individual V:5 (PKDF282) at *D15SA975* (78.56 Mb). CIB2 mutant alleles [c. 272T>C (p.Phe91Ser), c.297C>G (p.Cys99Trp) and c.297C>G (p.Ile123Thr)] co-segregate with NSHI phenotype in PKDF356, PKDF282, DEM4225 and family-802, respectively. The USH1 phenotype of family PKDF117 co-segregates with c.192G>C (p.Glu64Asp) mutation of *CIB2*. These four recessive mutations co-segregate with deafness or deaf-blindness while carriers have normal hearing.

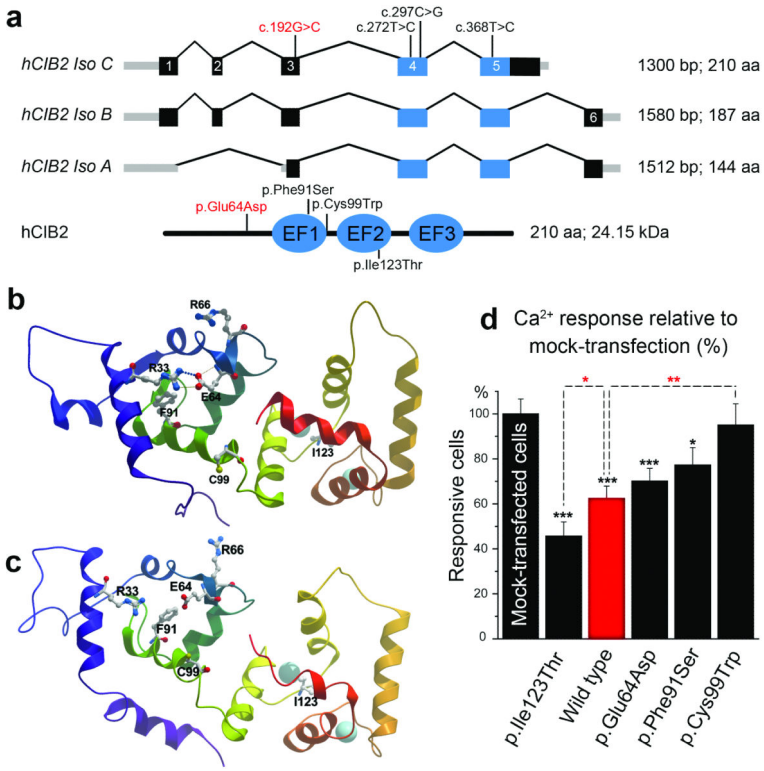

Figure 2.

CIB2 isoforms, molecular models, and functional effects of mutations. (**a**) Human *CIB2* has six exons encoding three isoforms. Non-coding, EF-hand domains and other coding regions of exons are denoted by grey, blue and black boxes, respectively. (**b**) Molecular models using template 1XO5.PDB crystal structure of Ca^{2+}-CIB1. (**c**) Model of CIB2 using a template for NMR structure of CIB1 bound to αIIβ integrin peptide.[7] (**b-c**) The backbone ribbon is color-coded blue (N-terminus) to red (C-terminus) and two Ca^{2+}-ions are blue spheres. (**d**) Ca^{2+} responses in COS-7 cells transfected with five different DsRed-tagged CIB2 constructs. Data normalized to average response of mock-transfections; shown as mean ± SE. Asterisks indicate statistical significance: ***, $p<0.001$; *, $p<0.05$. None of the four missense mutations resulted in noticeable changes of CIB2 distribution (not shown). p.Cys99Trp abolished CIB2's ability to decrease sensitivity of antagonist-induced Ca^{2+} release from the cell, while p.Ile123Thr enhanced this ability.

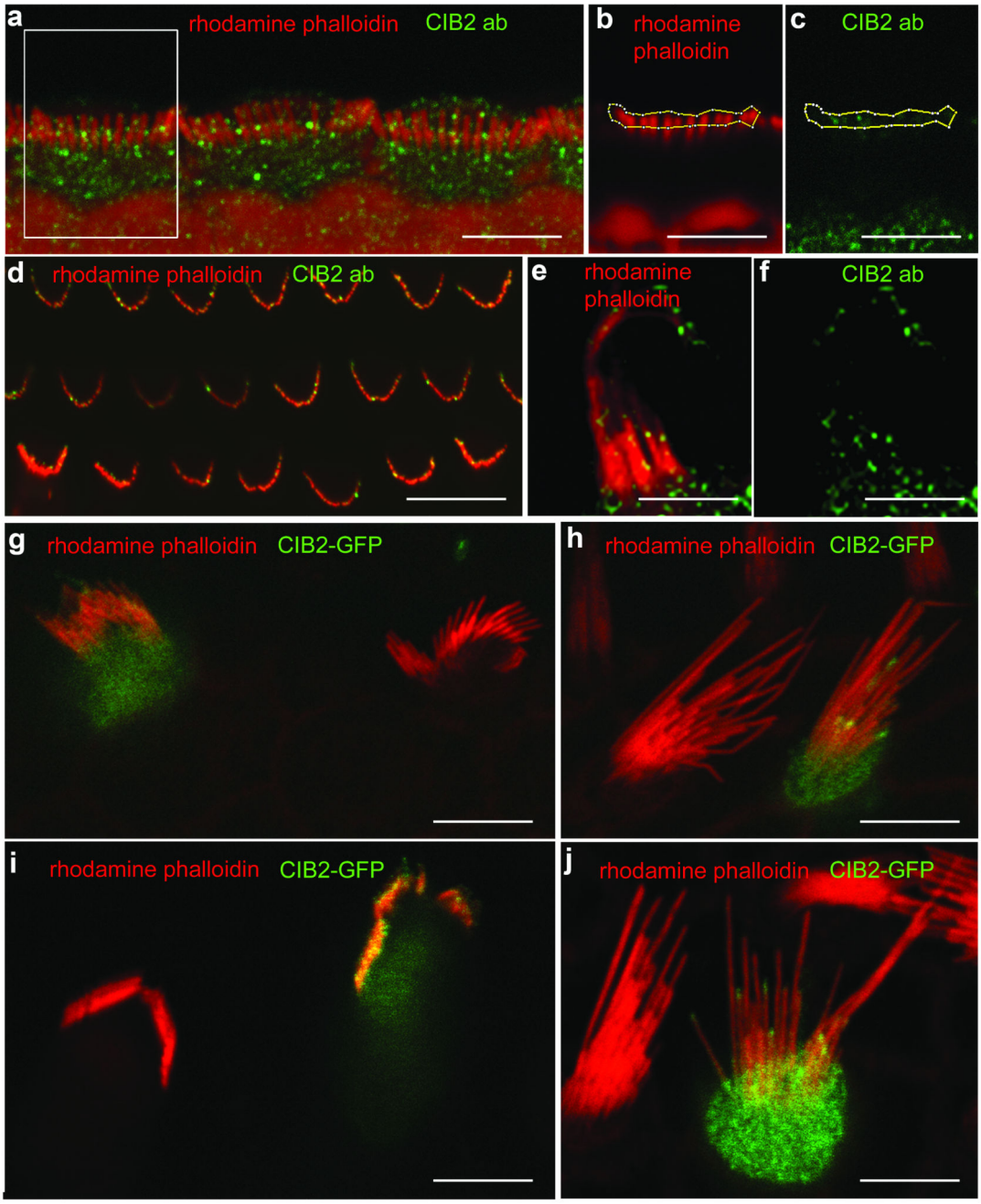

Figure 3.

CIB2 localization in hair cells of the organ of Corti and vestibular sensory epithelia. (**a** – **c**) Localization of CIB2 (green) in the inner hair cell stereocilia. F-actin is visualized by rhodamine-phalloidin (red). (**b, c**) shows boxed area in **a** at a higher magnification, separated in red (**b**, rhodamine-phalloidin) and green (**c**, CIB2) channels. The region of interest in **b** and **c** covered the tips of the second row stereocilia and was used to measure integrated intensity of fluorescent signal (Supplementary Table 6). (**d**) CIB2 (green) is present in stereocilia of outer hair cells. (**e, f**). CIB2 (green) in vestibular hair cell stereocilia cluster in patches around the actin core (red). Most of the CIB2 patches (**f**, green channel

alone) are observed near or at the tips of stereocilia. (**g, i**) Gene gun transfection of the organ of Corti hair cells with CIB2-GFP shows predominant targeting of CIB2 to stereocilia tips, particularly to the tips of the shorter row of inner (**g**) and outer (**i**) hair cell stereocilia. (**h, j**) Vestibular hair cell transfected with CIB2-GFP show greater concentration of CIB2-GFP (green) to the tips of shorter row stereocilia (red). Scale bars in all of the panels are 5 μm, except **d**. Scale bar in **d** is 10 μm.

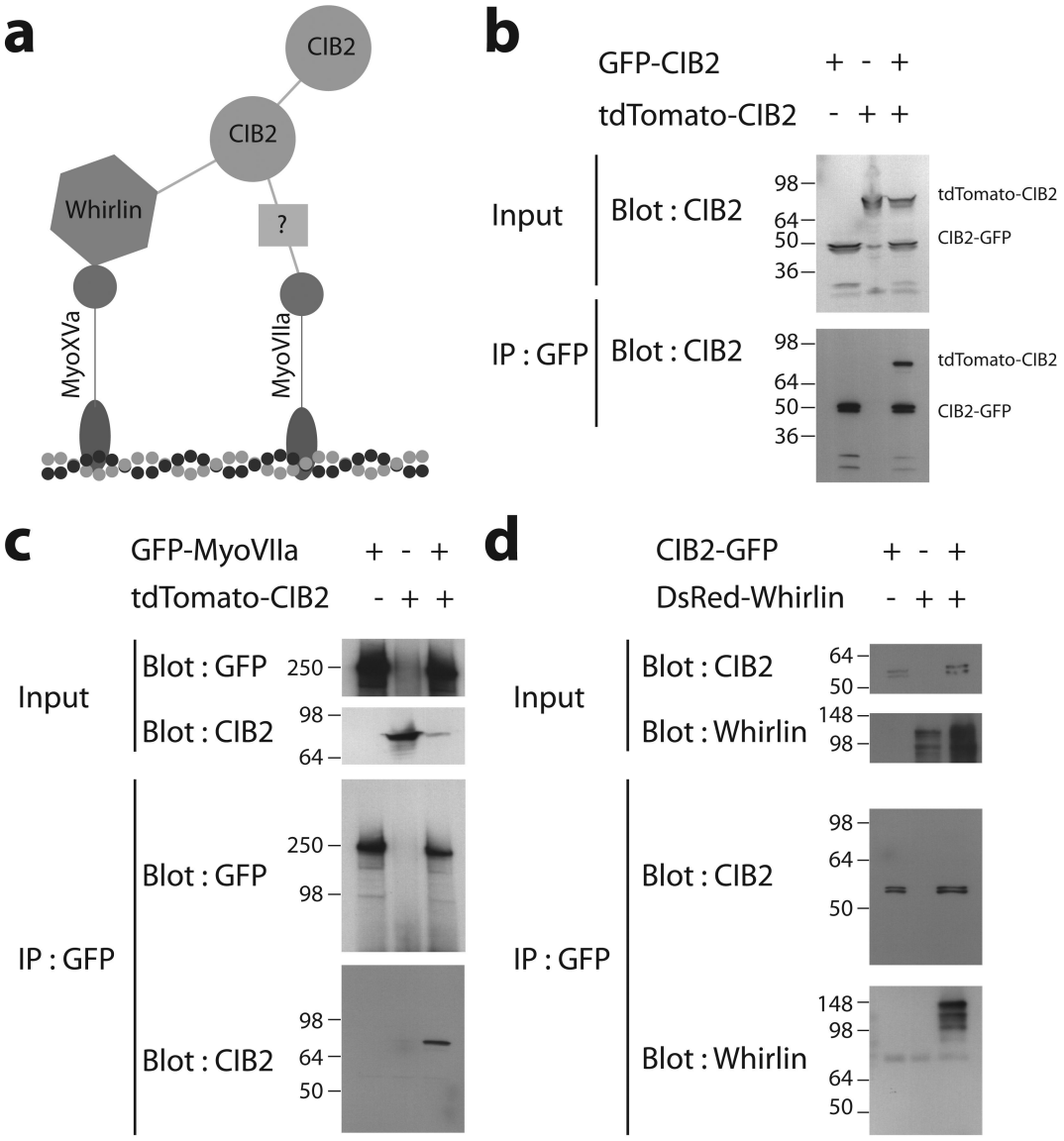

Figure 4.

CIB2 homodimerizes and also interacts with whirlin and myosin VIIa (**a**) Possible CIB2 interactome. Myosin VIIa might be interacting directly or through an intermediate protein. (**b**) CIB2 homodimerizes. Lysates from HEK293 cells transfected with CIB2-GFP and tdTomato-CIB2 expression constructs were co-immunoprecipitated with anti-GFP antibody. Precipitates were immuno-blotted with CIB2 and GFP antibody. (**c**) CIB2 and myosin VIIa interact. Lysates from HEK293 cells transfected with GFP-MyoVIIa and tdTomato-CIB2 constructs were co-immuno-precipitated with anti-GFP antibody. Precipitates were immuno-blotted with CIB2 and GFP antibodies. (**d**) CIB2 and whirlin interact. Lysates from HEK293 cells co-transfected with CIB2-GFP and DsRed-whirlin were co-immunoprecipitated with an anti-GFP antibody. Precipitates were immuno-blotted with CIB2 and whirlin antibodies. As negative control, we transfected CIB2-GFP either DsRed or tdTomato empty vectors and did not observe an interaction (Supplementary Fig. 10b-c). In this assay CIB2 does not

interact with harmonin, cadherin 23, protocadherin15-CD1, -CD2 and –CD3, Sans, usherin, vlgr1 or clarin-1.

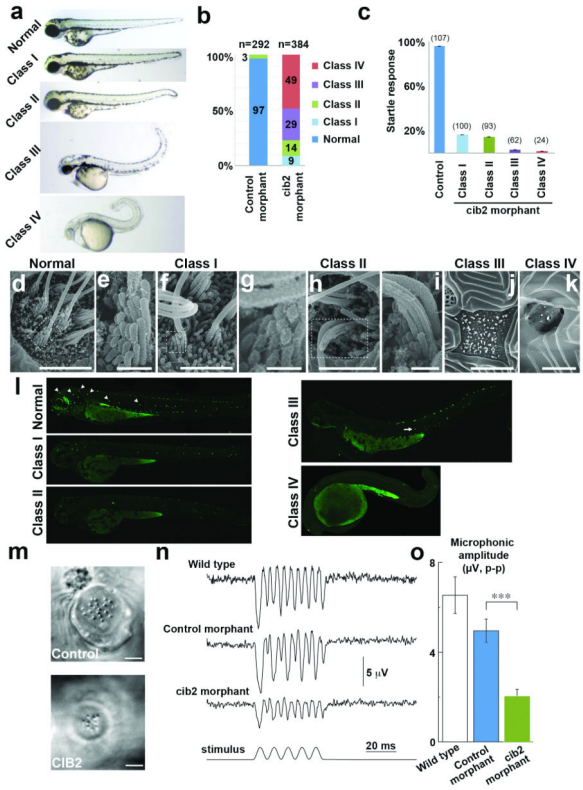

Figure 5.

Suppression of *cib2* expression produces developmental defects in zebrafish embryos. (**a - b**) Embryos injected with morpholino (MO) against *cib2* have developmental defects including micro-ophthalmia, curled tail, hypo-pigmentation and an edematous heart. (**c**) Acoustic startle reflex of 5-day-old morphants. A significant percentage of *cib2* MO injected larvae either did not respond to acoustic stimuli, indicating HI,[52] or were unable to remain upright while swimming, indicative of a balance defect, shown as mean ± SE (**d)** Scanning electronic microscopic (SEM) imaging revealed normal morphology of hair bundle in the neuromast. (**e**) Shows boxed area in **d** at a higher magnification. (**f - i**) SEM image revealed normal looking hair bundles in the neuromast cells in class I and class II morphants. (**g, i**) High-resolution imaging of neuromast present in the class I and class II morphants (boxed areas in **f** and **h**) showed the intact hair bundle links connecting the different rows. (**j**, **k**) Complete absence of neuromasts at the lateral lines of class III and IV *cib2* morphants. Scale bars: 5 μM for panel **j**, 3 μM for **d** and **f**, 2 μM for **h** and **k**, 500 nM for **e**, **g** and **i**. (**l – o**) Inhibition of microphonic potentials in zebrafish lateral line by *cib2* morpholino. (**l**) Comparison of FM1–43 labeling in larvae from all four classes at 72 hpf showed a marked reduction of uptake in *cib2* morphants. Arrow and arrowheads indicate the neuromast cells. (**m**), Bright field image of a neuromast in a zebrafish injected with control morpholino and with *cib2* morpholino. (**n**) Microphonic potentials in neuromasts of non-injected wild type fish (top trace), fish injected with control morpholino (second trace), and fish injected with *cib2* morpholino (third trace). The bottom trace indicates 2 μm peak-to-peak (p-p) stimulation. (**o**) Average peak-to-peak amplitude of microphonic potential in wild type,

control, and *cib2* morphants. Number of neuromasts: 17, wild type; 11, control; 20, CIB2. Data are shown as Mean ± SE. Asterisks indicate statistical significance: $p<0.001$.

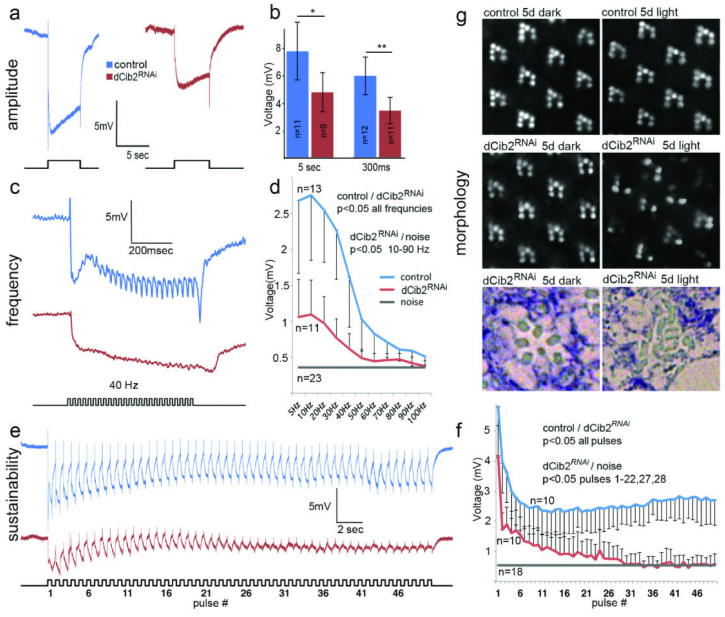

Figure 6.

Physiological and morphological changes in Drosophila dCib2 deficient retinas. (**a**) Electroretinogram illustrating the photo response to a 5 second white light pulse. *dCib2*^{RNAi} flies show a reduction in response amplitude of over 30% compared to control flies. (**b**) The amplitude reduction is significant (student *t*-test), with a p-value of 0.02 for 5 second pulses, and p=0.00005 for 300ms pulses. (**c**) An example of a 40Hz series (train) of light pulses illustrates that *dCib2*^{RNAi} flies are unable to follow fast trains of light pulses as well as control flies. At this frequency, the electric signal of control flies closely follows all light pulses, while *dCib2*^{RNAi} flies skip the majority of pulses and show only a very weak response to a few pulses. (**d**) Response amplitudes in *dCib2*^{RNAi} flies decreased to the noise levels at lower frequencies than do the responses in control flies. (**e**) In contrast to control flies, *dCib2*^{RNAi} flies are unable to maintain a persistent response during prolonged stimulation at a low frequency (1.7Hz). (**f**) On average, the response strength of dCIB2^{RNAi} flies becomes indistinguishable from noise levels after the first 22 pulses of stimulation. (**g**) Analysis of *dCib2*^{RNAi} retinas by water immersion (top two panel sets) or thin plastic sections (bottom panel set) reveal little to no differences from controls when raised in 12hr: 12hr light:dark cycles (not shown) or in complete darkness. However, significant degeneration is observed when flies are raised in constant light for 5 days, indicating that Cib2 is necessary to prevent light-induced retinal degeneration.